Supporting Information

Sato *et al.* 10.1073/pnas.0809148106

SI Text

Myocyte Experiments. Ventricular myocytes were enzymatically isolated from adult rabbit hearts. Briefly, hearts were removed from adult New Zealand White rabbits (2–3 kg) anesthetized with i.v. pentobarbital and perfused retrogradely in Langendorff fashion at 37 °C with nominally Ca-free Tyrode's solution containing ≈1.4 mg/ml collagenase (Type II; Worthington) and 0.1 mg/ml protease (type XIV; Sigma) for 25–30 min. After washing out the enzyme solution, the hearts were removed from the perfusion apparatus, and swirled in a culture dish. The Ca concentration was slowly increased to 1.8 mM, and the cells were stored at room temperature and used within 8 h. This procedure typically yielded ≈50% rod-shaped Ca-tolerant myocytes.

Myocytes were patch-clamped using the whole-cell configuration of the patch clamp technique. Patch pipettes (resistance 2–4 MΩ) were filled with pipette solution containing 110 nmM K-Aspartate, 30 nmM KCl, 5 nmM NaCl, 10 nmM Hepes, 0.1 nmM EGTA, 5 nmM MgATP, 5 nmM creatine phosphate, and 0.05 nmM cAMP (pH 7.2) with KOH. The cells were perfused by the standard Tyrode's solution contained 136 nmM NaCl, 5.4 nmM KCl, 0.33 nmM Na_2PO_4, 1.8 nmM $CaCl_2$, 1 nmM $MgCl_2$, 10 nmM glucose, and 10 nmM Hepes (pH 7.4) adjusted with NaOH. H_2O_2 (1 mM) was added directly to the bath superfusate. The voltage signals were measured with an Axopatch 200B patch-clamp amplifier controlled by a computer using a Digidata 1200 acquisition board driven by pCLAMP 8.0 software (Axon Instruments). The action potentials were elicited with 2-ms and 2- to 4-nA square pulses at various PCLs from 300 ms to 6 s. All experiments were performed at 34–36 °C.

Tissue Experiments. We studied 8 (3- to 6-year-old) female New Zealand White rabbits. The rabbits were anesthetized, the hearts were quickly removed, and the aorta was cannulated and perfused with oxygenated Tyrode's solution at a constant rate of 35 mL/min at 37 °C. Both atria were cut, and the endocardium and the mid-myocardium of right and the left ventricles (excluding the epicardium of the anterior left ventricular wall) were cryoablated by placing a 7-cm SurgiFrost probe (ATS Medical). The probe was placed in the LV cavity and its temperature decreased to −56 °C for 5 min to ablate the RV and posterior LV while the epicardium was protected by perfusing it with warm (37 °C) oxygenated Tyrode's solution. Sites of myocardial necrosis were identified with 1% triphenyl tetrazolium chloride (TTC) perfusion through the aorta. Transmural sectioning identified the areas of necrosis with the preservation of a thin rim (<1 mm) of viable epicardial tissue.

Two widely spaced electrodes were positioned, one at the LV base and the other at the apex, to record a "pseudoelectrocardiogram," (ECG) as previously described (1). The hearts were stained with the voltage-sensitive fluorescent dye RH 237, excited at 532 nm with epifluorescence collected by a CCD camera (CA-D1–0128T; Dalsa) through a 715-nm long-pass filter (Nikon). We used Blebbistatin (Biomol) (10 μM) as an excitation–contraction uncoupler for stable optical and microelectrode recordings. H_2O_2 (0.2–1 mM) was perfused, and spontaneous as well as pacing induced ventricular tachycardia and fibrillation (VT and VF respectively) were recorded.

Computational Simulations. ***Isolated cell.*** Voltage of isolated myocytes is described by the following differential equation:

$$dV/dt = (-I_{\text{ion}} + I_{\text{sti}})/C_m, \qquad \textbf{[s1]}$$

where V is the membrane potential and $C_m = 1\ \mu\text{F/cm}^2$. I_{ion} is the total membrane ionic current, which is described below. I_{sti} is the stimulation current, which was a pulse of strength 40 $\mu\text{A/cm}^2$ and duration 1 ms. Eq. **s1** was numerically solved by using the Euler method with an adaptive time step varying from 0.01 to 0.1 ms.

Simulation of stochastic ion channel fluctuations. To simulate the stochastic channel fluctuations, we modified I_{ks} in the AP model by modeling the gating variable x_{s1} using a Langevin equation developed by Fox (2), i.e.,

$$\frac{dx_{s1}}{dt} = k_+ (1 - x_{s1}) - k\_x_{s1} + \eta(t), \qquad \textbf{[s2]}$$

where η is the stochastic noise with the following correlation relation:

$$\langle \eta(t)\eta(t') \rangle = \frac{k_+(1 - x_{s1}) + k\_x_{s1}}{N}\, \delta(t - t') \qquad \textbf{[s3]}$$

and $k_+ = x_s^\infty$ and $k_- = 1/\tau_{xs1} - k_+$.

1D cable model. The partial differential equation to describe the membrane potential V in the 1D cable is:

$$\frac{\partial V}{\partial t} = (-I_{\text{ion}} + I_{\text{sti}})/C_m + D\,\frac{\partial^2 V}{\partial x^2}, \qquad \textbf{[s4]}$$

where D is the diffusion constant, which was set to 0.001 cm^2/ms. With this diffusion constant, the conduction velocity is ≈55 cm/s. No-flux boundary conditions were used for Eq. **s4**. Eq. **s4** was discretized with $\Delta x = 0.15$ mm (approximately the length of a myocyte).

2D tissue model. The partial differential equation to describe the membrane potential V in the homogeneous 2D tissue is

$$\frac{\partial V}{\partial t} = -I_{\text{ion}}/C_m + D\left(\frac{\partial^2 V}{\partial x^2} + \frac{\partial^2 V}{\partial y^2}\right). \qquad \textbf{[s5]}$$

No-flux boundary conditions were used. $D = 0.001$ cm^2/ms. $\Delta x = \Delta y = 0.15$ mm.

Rabbit ventricle model. The governing partial differential equation of voltage for the anatomical rabbit ventricles is (3–5):

$$\partial V/\partial t = -I_{\text{ion}}/C_m + \nabla\cdot\tilde{D}\nabla V, \qquad \textbf{[s6]}$$

where $\tilde{D}$ is the diffusion tensor. Due to fiber structure in the anatomical ventricles, each location has 3 principal directions: one along the myocardial fiber $\hat{\alpha}$ (a unit vector), the second, orthogonal to the fiber direction and lying in the myocardial sheet plane $\hat{\beta}$, and the third, orthogonal to the above 2 vectors, in the cross-sheet direction $\hat{\gamma}$. In the local or fiber coordinate system constructed by the 3 orthogonal vectors, the diffusion tensor is diagonal, i.e.,

$$D = \begin{pmatrix} D_{//} & 0 & 0 \\ 0 & D_\perp & 0 \\ 0 & 0 & D_\perp \end{pmatrix}, \qquad \textbf{[s7]}$$

where $D_{//} = 0.001$ cm^2/ms is the diffusion constant along the fiber direction and $D_\perp = 0.00025$ cm^2/ms is the diffusion constants in the transverse directions. The diffusion tensor in Eq. **s6** then can be calculated as

$$\tilde{D} = ADA^T, \qquad \textbf{[s8]}$$

where $A = (\hat{\alpha}, \hat{\beta}, \hat{\gamma})$ is the transformation matrix and A^T is the transpose matrix of A. For more details on this transformation, see ref. 5. The rabbit ventricular anatomy and fiber-orientation data were generously supplied by the Cardiac Mechanics Research Group at the University of California at San Diego. The ventricles were discretized with a spatial resolution of $\Delta x = \Delta y = \Delta z = 0.155$ mm, resulting in >3,600,000 computational grid points (4).

Calculation of PseudoECG. PseudoECG was calculated by using the following equation (3, 5):

$$\Phi_e(x', y', z') = \iiint_{\text{Volume}} \sum_{i=1}^{3} \sum_{j=1}^{3} \tilde{D}_{ij} (\nabla V)_j (\nabla (1/R))_i dx dy dz, \qquad \textbf{[s9]}$$

where $R = \sqrt{(x - x')^2 + (y - y')^2 + (z - z')^2}$ and (x', y', z') is the location of the electrode, and (x,y,z) is the location of electrical source in the tissue. $\tilde{D}_{ij}$ is an element of the 3×3 matrix $\tilde{D}$. The integration of Eq. **s9** is reduced to $\Phi_e(x',y',z') = D\int_L (\nabla V)(\nabla(1/R))dx$, where L is the length of the cable, and for the homogeneous 2D tissue to $\Phi_e(x',y',z') = D\iint_A (\nabla V)(\nabla(1/R))dxdy$, where A is the total area of the tissue.

Initial conditions for tissue simulations. Due to Na^+ and Ca^{2+} accumulation, it takes many pacing beats for the model to develop into a stationary state for a specific pacing cycle length. To save computation time, especially for 2D tissue and anatomical ventricles, we paced a single cell into its stationary state that then was used as initial conditions for all other cells in the tissue.

Numerical and simulation methods. The partial differential equations were numerically solved using the operator splitting method (6) with a time step varying from 0.01 to 0.1 ms. The space step was set to 0.015 cm for 1D cable and 2D tissue and to 0.0155 cm for the anatomical heart. Simulations of isolated myocytes, 1D cable, and 2D tissue were carried out on single-processor computers. Simulations of the anatomical ventricles were carried out on a 32-node high-performance computing cluster. Each node has 2 dual-core AMD Opteron 2.0-GHz CPUs and 4-GB RAM. The code was parallelized by using the Message-Passing Interface (MPI). Simulations were done by using 32 CPUs. To simulate 1 s of electrical activity in the heart, it takes ≈6.2 × 32 CPU hours. All computer programs were coded in C++.

AP models. We modified the AP model originally developed by our group (7) to obtain certain AP properties. We were not able to induce EADs in the original model simply by increasing the inward currents [by increasing the maximum conductance of the L-type Ca^{2+} current (I_{Ca}) or the Na^+–Ca^{2+} exchange current] or decreasing the outward K^+ currents. To induce EADs, we modified the rate constant in the Markovian model of I_{Ca} to cause steeper activation and inactivation kinetics, increased the maximum conductance of the L-type Ca^{2+} current, and reduced the maximum conductance of I_{Ks}. The major changes are summarized in the first model described below. Other models used in this study are modifications from the first model and are also described below.

In the first AP model (for the simulations in Figs. 1–3, and Figs. S2, S4, and S5), the total ionic current was: $I_{ion} = I_{Na} + I_{to,f} + I_{to,5} + I_{Ks} + I_{NaK} + I_{Ca} + I_{NaCa}$. The mathematical formulations of these currents was the same as in the paper by Mahajan *et al.* (7), except that $I_{to,s}$ was changed to $I_{to,s} = g_{to,s}X_{to,s}(0.5Y_{to,s} + 0.5R_s)(V - E_K)$ in which R_s is governed by $dR_s/dt = R_s^\infty - R_s/\tau R_s$ with $R_s^\infty = 1/[1 + e^{(V+33.5)/10}]$ and $\tau_{Rs} = 2300/[1 + e^{(V+60)/10}] + 720$. We also modified the rate constants of the Markovian formulation of the L-type Ca^{2+} channel as follows: $P_0^\infty = 1/[1 + e^{-(V-4.36)/6.8}]$, $s_1 = 0.367f(c_p)$, $k_1 = 0.0298f(c_p)$, $k_3 = e^{-(V+50)/10}/3[1 + e^{-(V+50)/10}]$, $T_{Ca} = 190/[1 + (c_p/\bar{c}_p)^4]$, + 10, $P_r = e^{-(V+30)/0.05}/[1 + e^{-(V+30)/0.05}]$, $P_s = 1/[1 + e^{-(V+40)/10}]$, $k_2 = k_1(s_2/s_1)(r_2/r_1)$, $k_2' = k_1'(s_2'/s_1')(r_2/r_1)$ and $g_{SR}(V) = \bar{g}_{SR}e^{-0.346(V+30)}/(1 + e^{-0.346(V+30)})$. The parameter changes are summarized in Table S1.

In the second AP model (for the simulations in Fig. 4, and Fig. S6), we added the nonspecific Ca^{2+}-activated current (I_{nsCa}) to the AP model described above, i.e., $I_{ion} = I_{Na} + I_{to,f} + I_{to,s} + I_{Kr} + I_{Ks} + I_{K1} + I_{NaK} + I_{Ca} + I_{NaCa} + I_{nsCa}$. I_{nsCa} was adopted from the Luo and Rudy model (8) with the following parameter changes: $P_{ns(Ca)} = 0.00000007$ and $K_{m,ns(Ca)} = 0.5$ μM.

In the third AP model (for the simulations in Fig. 5), the parameters changed from the second model as: $g_{Ca} = 1{,}000$ mmol/(cm C), $\tau_{po} = 0.3$ ms, $s_6 = 7.1$ ms^{-1}, $V_{th} = -15$ mV, $g_{to,f} = 0.4$mS/μF, $g_{to,s} = 0.006$ mS/μF, $g_{K1} = 0.3$ mS/μF, $g_{Kr} = 0.027$ mS/μF, $g_{Ks} = 0.4$ mS/μF, $g_{NaCa} = 1.5$ mS/μF, $g_{NaK} = 6.1$ mS/μF, $P_{ns(Ca)} = 0.000000105$, and $K_{m,ns(Ca)} = 0.5$ μM.

The fourth model that was used for the simulations shown in Fig. S3 was modified from the first model as: $g_{Ca} = 655.2$ mmol/(cm C), $g_{Ks} = 0.768$ mS/μF, and $g_{Kr} = 0.01$ mS/μF.

1. Ono N, *et al.* (2007) Spontaneous atrial fibrillation initiated by triggered activity near the pulmonary veins in aged rats subjected to glycolytic inhibition. *Am J Physiol* 292:H639–H648.
2. Fox RF (1997) Stochastic versions of the Hodgkin–Huxley equations. *Biophys J* 72:2068–74.
3. Xie F, *et al.* (2004) A simulation study of the effects of cardiac anatomy in ventricular fibrillation. *J Clin Invest* 113:686–93.
4. Baher A., *et al.* (2006) Short-term cardiac memory and mother rotor fibrillation. *Am J Physiol* 292:H180–H189.
5. Panfilov AV, Holden AV (1997) *Computational Biology of the Heart* (Wiley, New York).
6. Qu Z, Garfinkel A (1999) An advanced numerical algorithm for solving partial differential equation in cardiac conduction. *IEEE Trans Biomed Eng* 49:1166–1168.
7. Mahajan A, *et al.* (2008) A rabbit ventricular action potential model replicating cardiac dynamics at rapid heart rates. *Biophys J* 94:392–410.
8. Luo CH, Rudy Y (1994) A dynamical model of the cardiac ventricular action potential: I. Simulations of ionic currents and concentration changes. *Circ Res* 74:1071–1096.

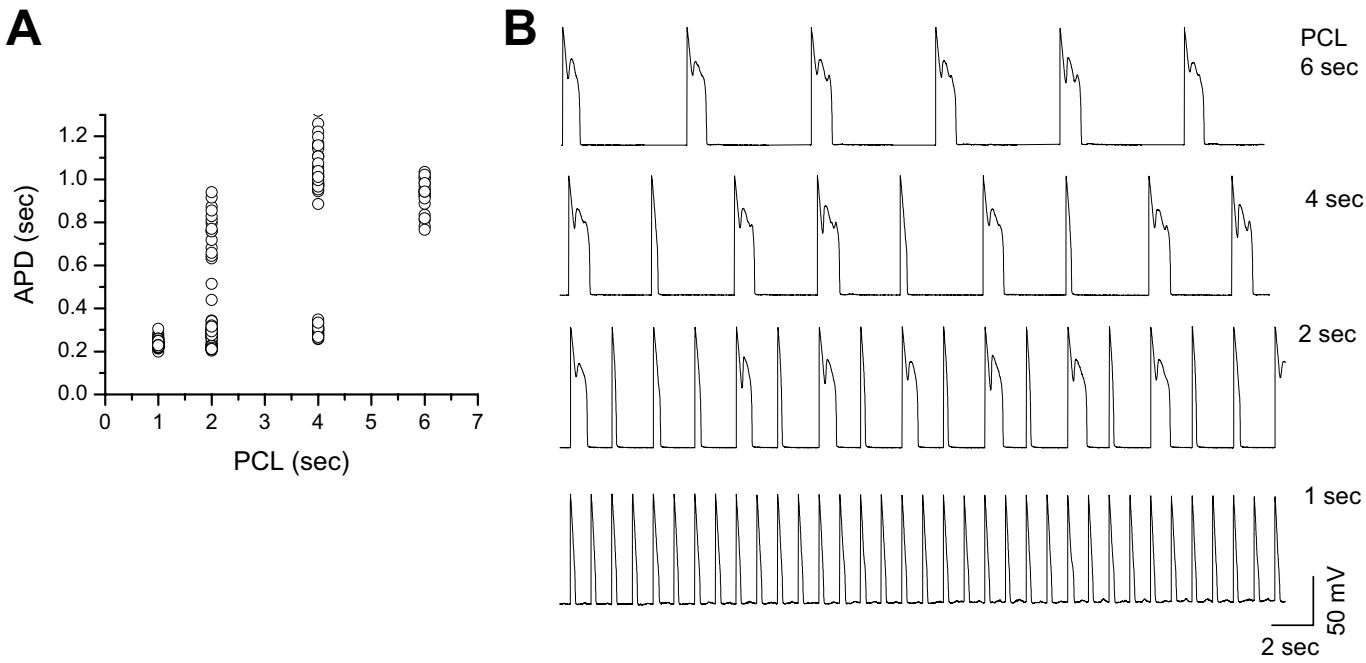

Fig. S1. APD vs. PCL (*A*) and voltage recordings (*B*) from a myocyte exposed to 1 mM H_2O_2, the same as in Fig. 1*A*.

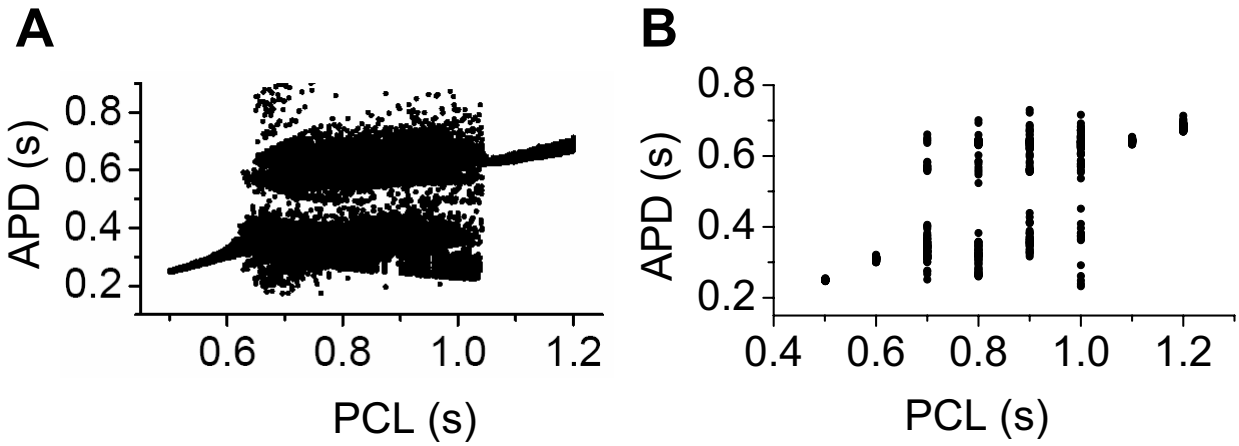

Fig. S2. APD versus PCL from the action potential model as in Fig. 1*B* but in the presence of random channel fluctuations with dense sampling in PCL (*A*) and sparse sampling as in the experiment shown in Fig. 1*A* (*B*).

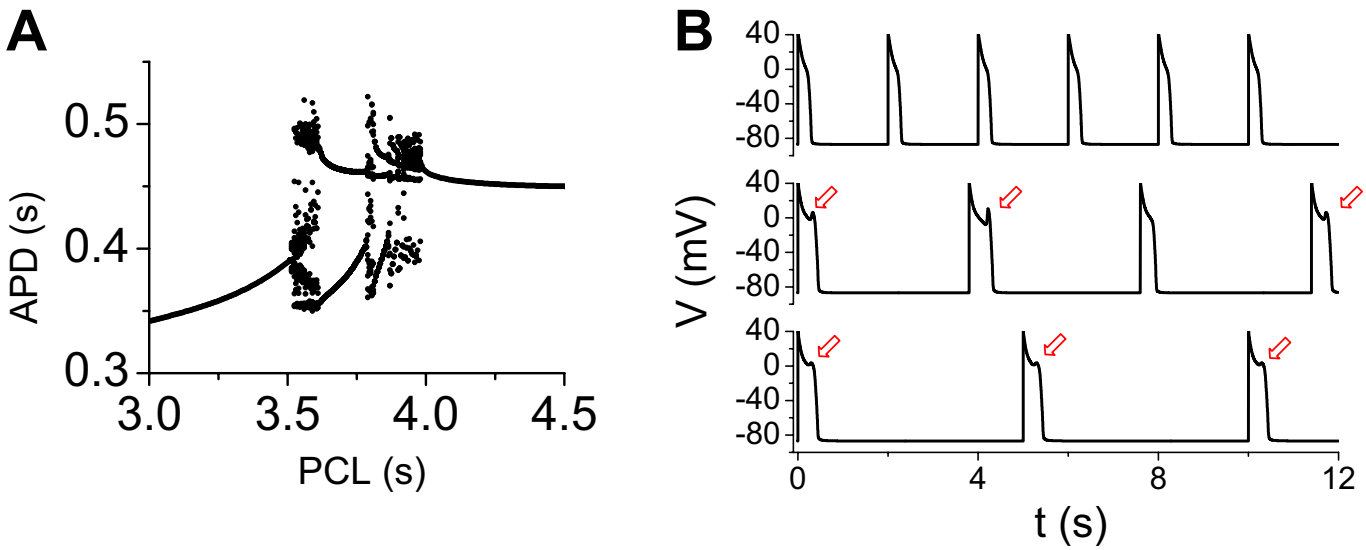

Fig. S3. Chaotic EADs occur at slow pacing rates in a single-cell model (the fourth AP model). (*A*) Bifurcation diagram showing APD vs. PCL. (*B*) Voltage traces from different PCLs: PCL = 2 s (*Top*), PCL = 3.8 s (*Middle*), and PCL = 5 s (*Bottom*).

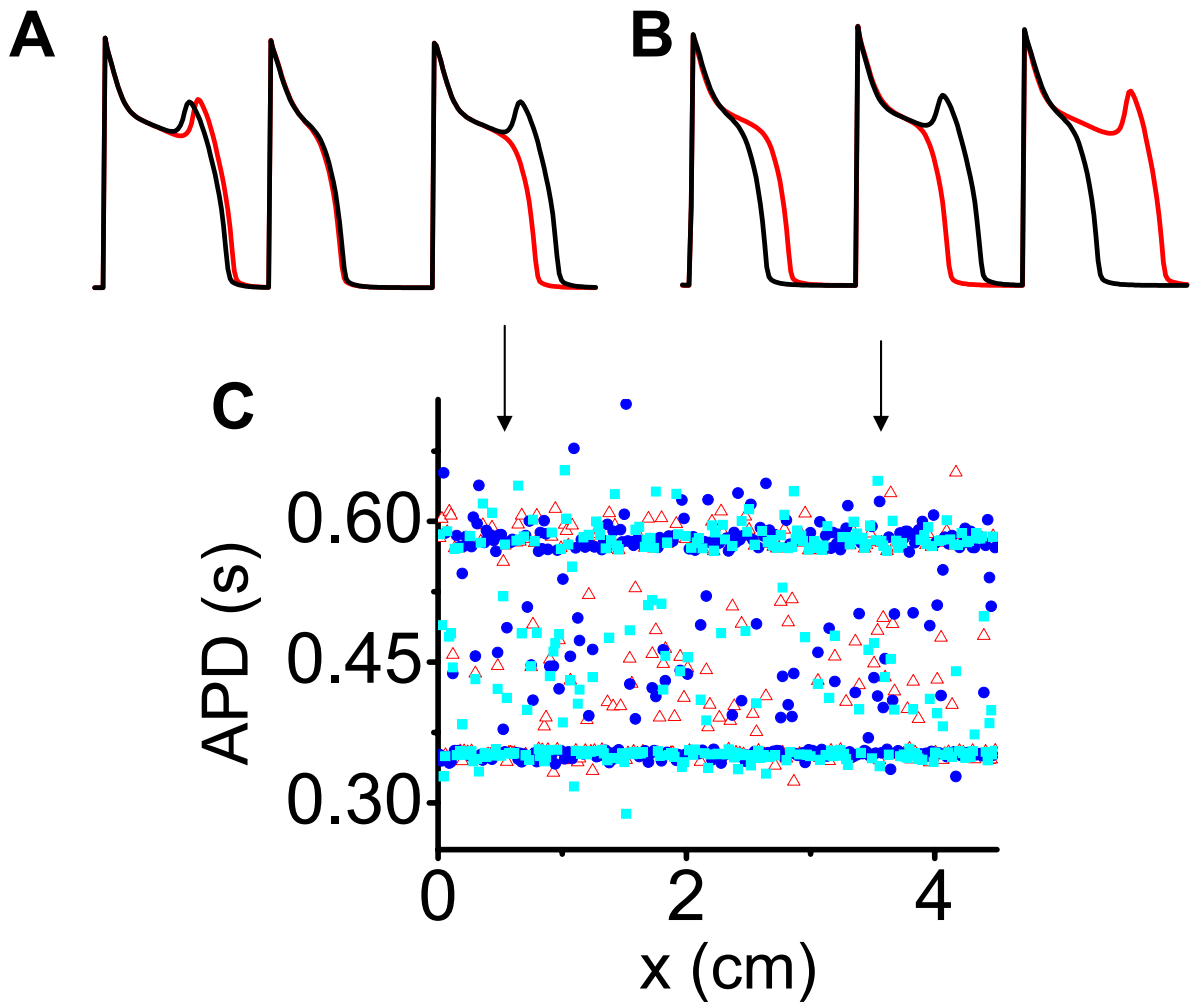

Fig. S4. Action potentials and APD distribution in a 1D uncoupled cable. (*A* and *B*) Voltage traces from 2 neighboring cells (red and black) in 2 different locations (indicated by the 2 arrows) from a 1D cable of uncoupled cells. (*C*) The same plot of Fig. 3*A* in the main text. The initial conditions of the cells were slightly different from each other. The 3 consecutive beats were recorded after many pacing beats.

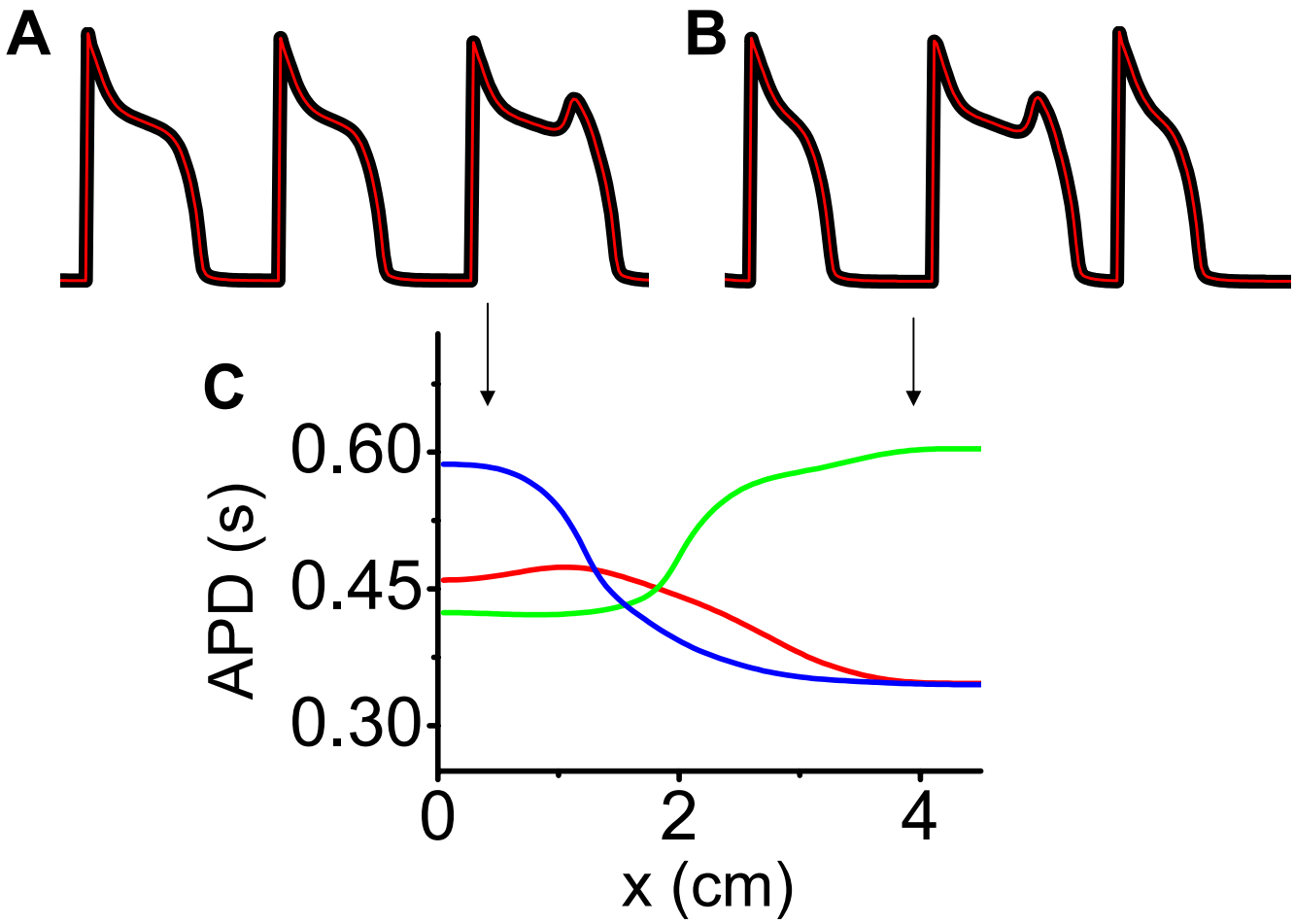

Fig. S5. Action potentials and APD distribution in a 1D coupled cable. (*A* and *B*) Voltage traces from 2 neighboring cells (red and black) in 2 different locations (indicated by the 2 arrows) from a 1D cable of electrotonically coupled cells. (*C*) The same plot as Fig. 3*B* in the main text. The initial conditions of the cells were slightly different from each other. The 3 consecutive beats were recorded after many pacing beats.

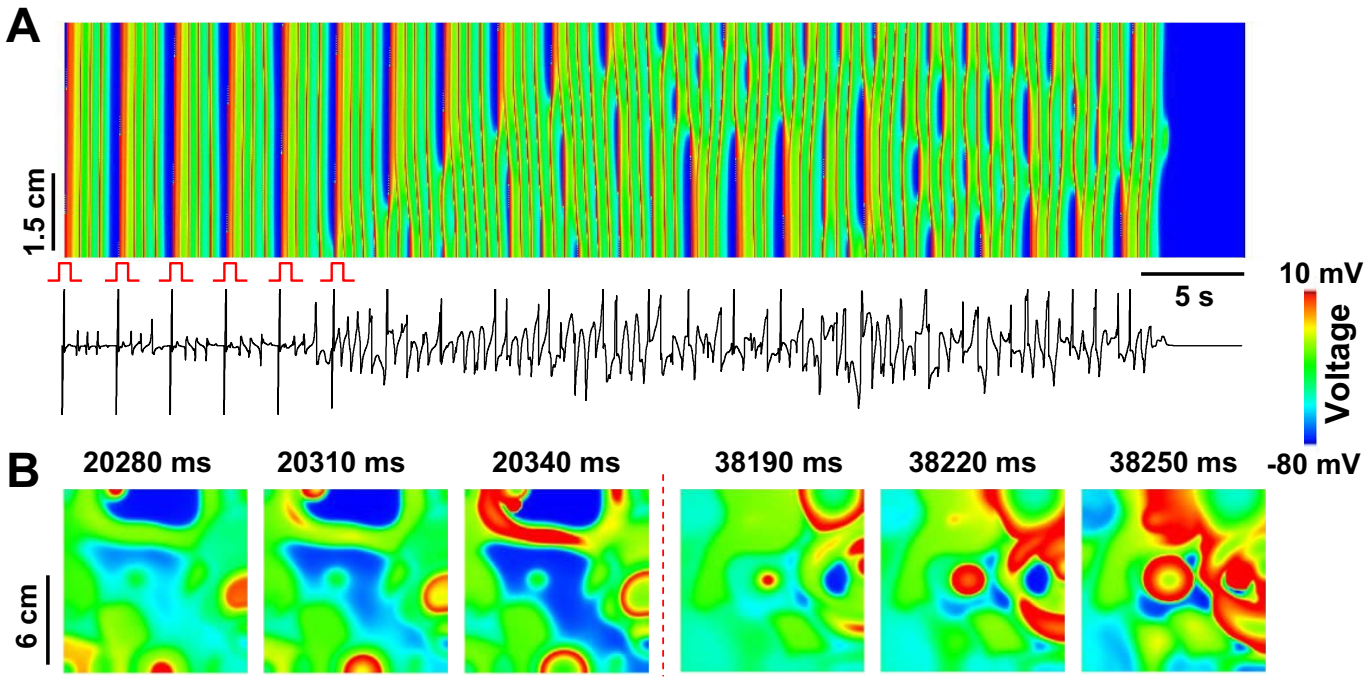

Fig. S6. Multifoci arrhythmias in homogeneous tissue models. (*A*) (*Upper*) Space (*y* axis) and time (*x* axis) plot of voltage in a 4.5-cm homogeneous 1D cable paced at one end for 6 beats (as indicated) showing the formation of multiple floating foci due to a spatial instability. (*Lower*) PseudoECG showing polymorphic tachycardia, terminated spontaneously due to the finite size of the cable. (*B*) Voltage snapshots of 2 episodes (from 20,280 to 20,340 ms and from 38,190 to 38,250 ms) of multiple floating foci from a simulation in a 12 × 12-cm homogeneous 2D tissue.

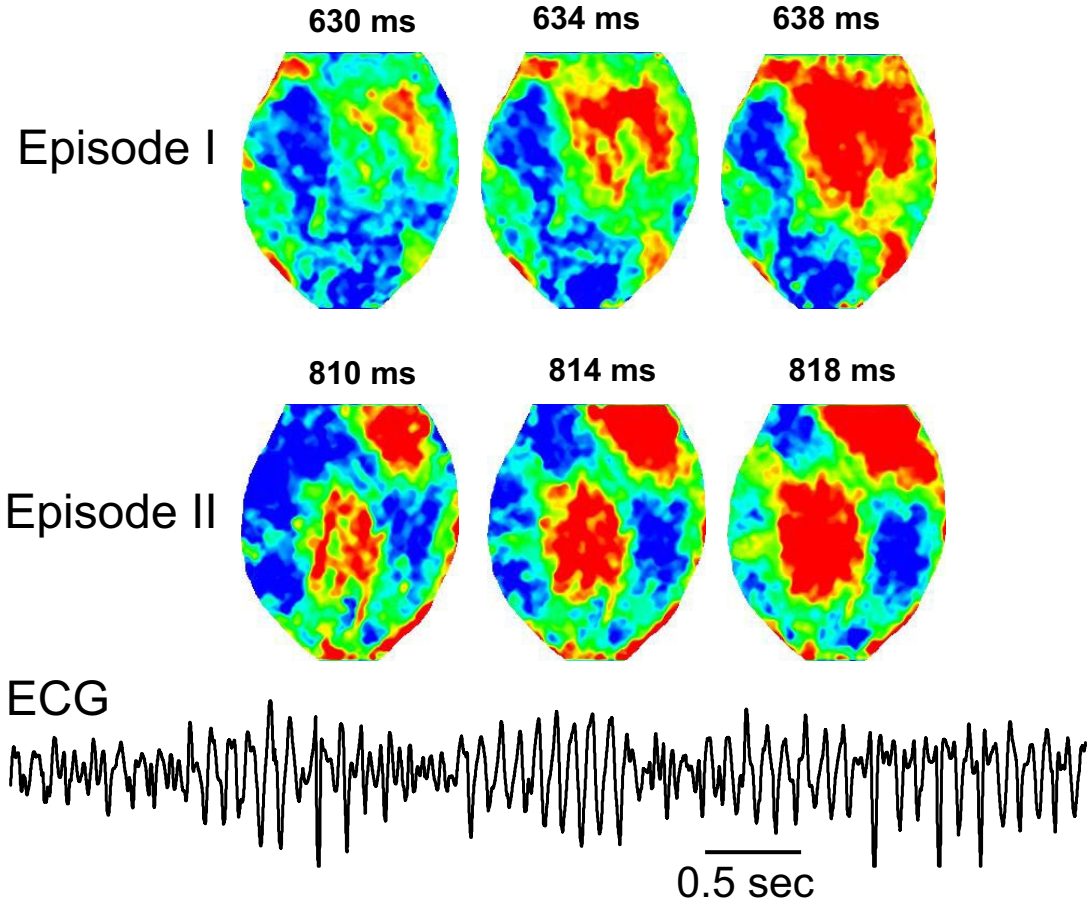

Fig. S7. Multifoci arrhythmias in a cryoablated heart. (*Upper*) Voltage snapshots on the epicardical surface of a rabbit heart during exposure to 1 mM H2O2, showing 2 episodes of multiple EAD-induced foci (from 630 to 638 ms with 1 foci and from 810 to 818 ms with 2 focus) in a cryoablated heart. (*Lower*) Pseudoelectrocardiogram from the same simulation showing Torsade de pointes.

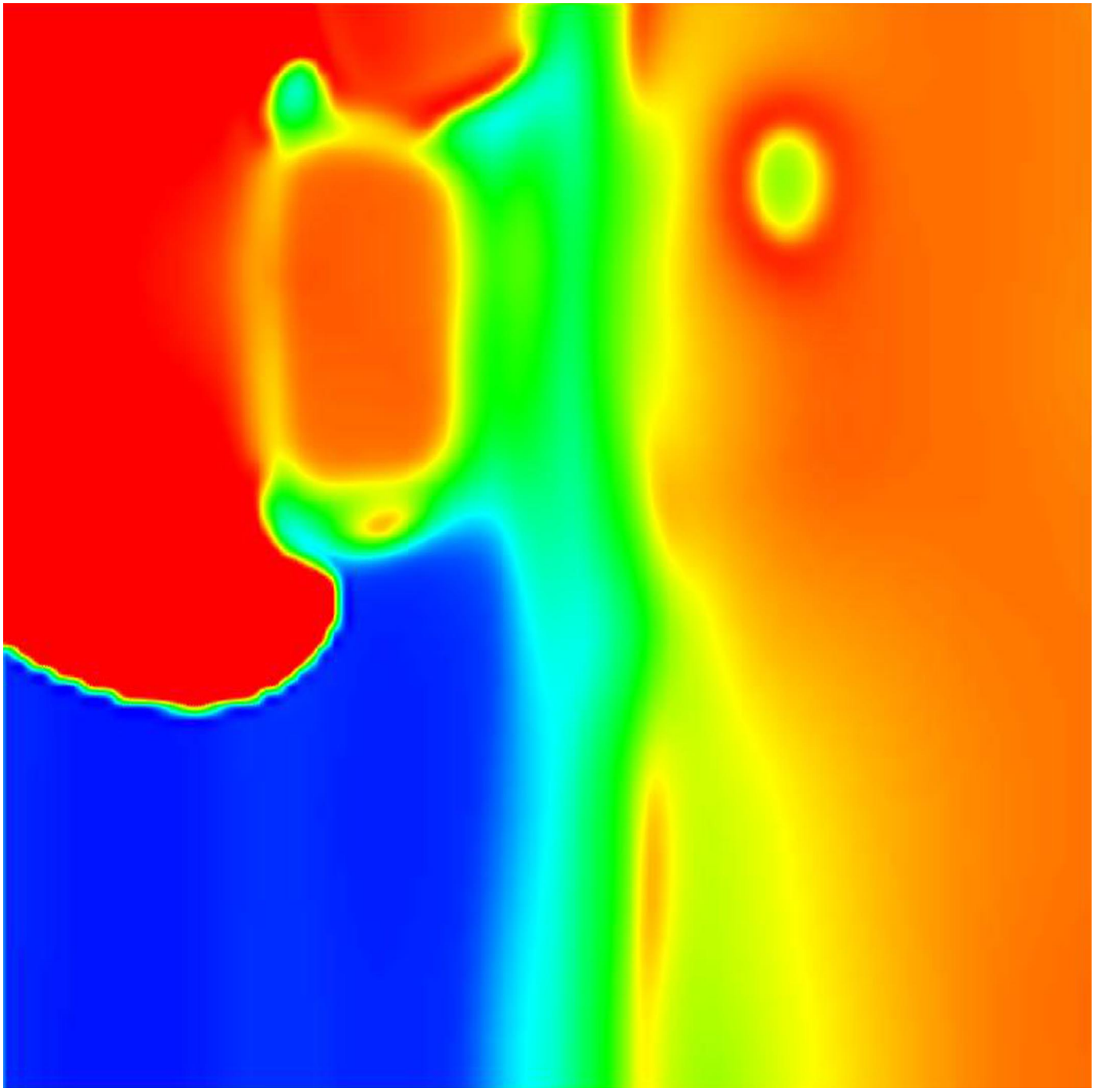

Movie S1. Reentry induction due to chaos desynchronization in a homogeneous 2D tissue.

Movie S1 (MOV)

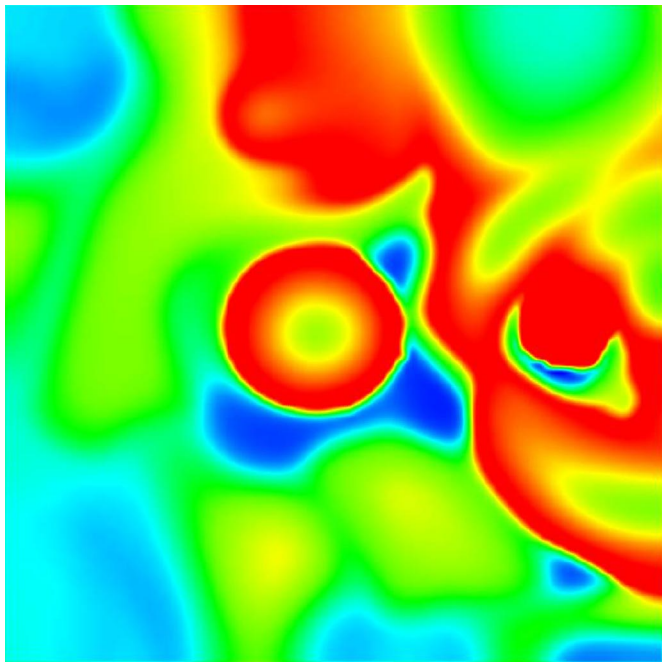

Movie S2. Multifoci arrhythmias in a homogeneous 2D tissue.

Movie S2 (MOV)

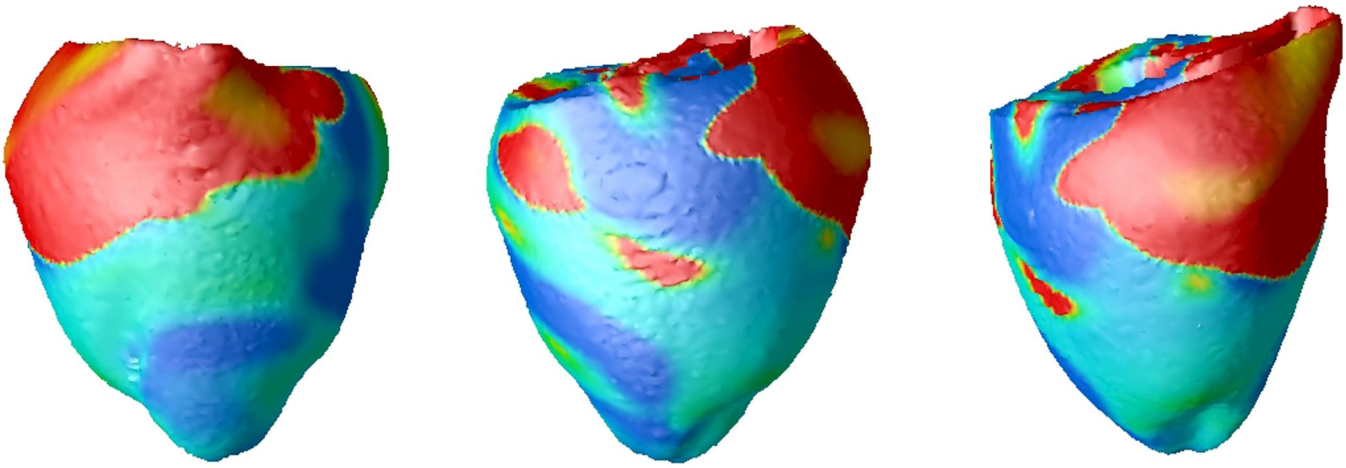

Movie S3. Multifoci arrhythmias in an anatomic rabbit ventricle model.

Movie S3 (MOV)

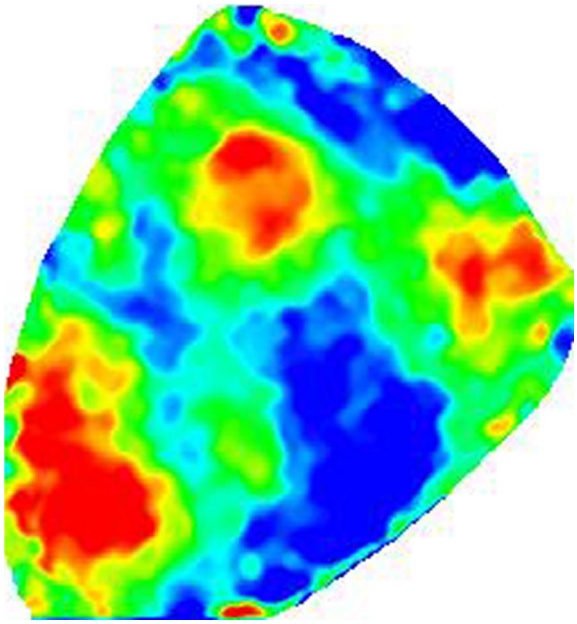

Movie S4. Multifoci arrhythmias in a rabbit heart.

Movie S4 (MOV)

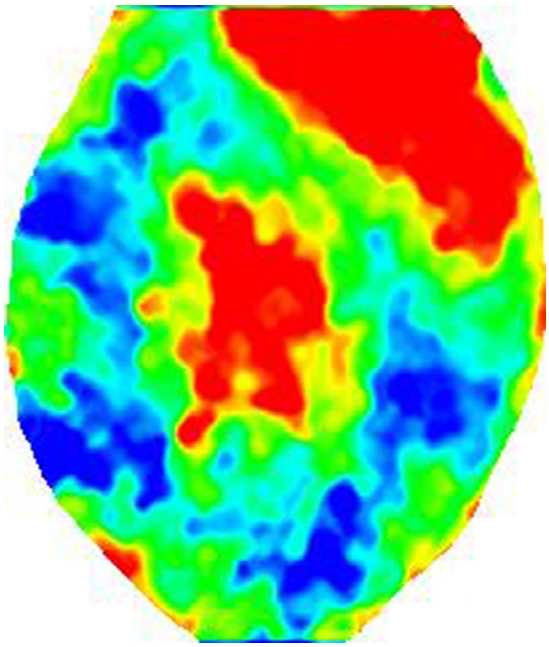

Movie S5. Multifoci arrhythmias in a cryoablated rabbit heart.

Movie S5 (MOV)

Table S1. Parameters that are changed from the original model

Parameter	Definition	Value
P_{Ca}	Constant	0.00054 cm/s
g_{Ca}	Strength of Ca current flux	546 mmol/(cm C)
$\bar{g}_{Ca}$	Strength of local Ca flux due to L-type Ca channels	9,998.6 mmol/(cm C)
$\bar{g}_{SR}$	Strength of local Ca flux due to RyR channels	23,692 mmol/(cm C)
k_p^0	Threshold for Ca-induced inactivation	5.0117 μM
$\bar{c}_p$	Threshold for Ca dependence of transition rate k_6	4.0 μM
τ_{po}	Time constant of activation	0.35 ms
r_1	Opening rate	0.41 ms^{-1}
r_2	Closing rate	2.7 ms^{-1}
$s_1^{'}$	Inactivation rate	0.00175 ms^{-1}
$k_1^{'}$	Inactivation rate	0.00413 ms^{-1}
s_2	Inactivation rate	0.000377 ms^{-1}
$s_2^{'}$	Inactivation rate	0.000687 ms^{-1}
T_{Ba}	Time constant	671.082 ms
g_{RyR}	Release current strength	3.0 sparks cm^2/mA
$g_{to,f}$	Peak $I_{to,f}$ conductance	0.055 mS/μF
$g_{to,s}$	Peak $I_{to,s}$ conductance	0.08 mS/μF
g_{K1}	Peak I_{K1} conductance	0.36 mS/μF
g_{Kr}	Peak I_{Kr} conductance	0.006 mS/μF
g_{Ks}	Peak I_{Ks} conductance	0.153 mS/μF
v_{up}	Strength of uptake	0.8 μM/ms
B_{ATP}	Total concentration of ATP-binding sites	5,000.0 μmol per l cytosol
K_{ATP}	Dissociation constant for ATP-binding sites	200.0 μM